Lattice Design of the LANL Spallation-Source Compressor Ring*

Barbara Blind, Andrew J. Jason, and Filippo Neri
Los Alamos National Laboratory
AT-3, MS H811, Los Alamos, NM 87545, USA

Abstract

A new compressor ring for 790-MeV protons is proposed at Los Alamos National Laboratory to provide 1 MW of beam power for a spallation-neutron source. The design has unit-transfer-matrix achromatic arcs. Bunching, beam-control, and extraction elements reside in dispersionless straight sections. The arc symmetry and further high-order corrections maximize tune space available to the beam. The ring-injection scheme uses direct H^- injection and care is taken in disposing of the unstripped and partially stripped beams. The lattice design allows for transverse phase-space painting to maximize particle storage, as well as minimize stored-beam foil traversals.

I. INTRODUCTION

The ring is just one component of a proposed upgrade of the Los Alamos Meson Physics Facility (LAMPF) [1], designed to deliver 1 MW of beam power to two target stations operating at 40 Hz and 20 Hz, respectively. The 1.2-ms LAMPF pulse must be delivered to the ring in an irregular pattern 60 times per second; pulsed devices must hence operate at 120 Hz. Chopped beam (436 ns on, 235 ns off) is injected into the 671-ns-circumference ring for about 1790 turns. Beam bunches are superimposed by direct H^- injection. A gap is maintained by an rf system consisting of twelve cavities operating at first through fifth ring harmonic to produce a barrier bucket. At extraction the gap is 168 ns, sufficient for the fast ferrite kicker to rise and cleanly remove the 503-ns beam bunch from the ring in single-turn extraction.

A ring energy of 790 MeV was chosen, even though the LAMPF accelerator nominally delivers H^- of 800 MeV, because beam energy will be swept with the last 805-MHz side-coupled-linac tank by ±4 MeV during injection.

The ring circumference of 168.886 m was chosen so that the revolution frequency for 790-MeV protons is a subharmonic of 805 MHz; additionally, all five barrier-bucket rf harmonics are subharmonics of 805 MHz. A barrier bucket was chosen for its ability to keep the gap beam free, avoiding extraction losses as well as a possible e-p instability, and because it allows maximum beam capture and provides a bunching factor (average current/peak current) of 0.55, compared to 0.25 for a first-harmonic cavity. The beam emittance necessary to keep the space-charge tune depression below a certain value is inversely proportional to this bunching factor.

II. RING-DESIGN OVERVIEW

The ring is described in Table 1 and shown in Figure 1;

Table 1
Ring Design Parameters

Energy (MeV)	790
Circumference (m)	168.886
Repetition Rate (Hz)	40 + 20
Particles Per Pulse	$1.32 \cdot 10^{14}$
Number of Cells in Achromatic Arc	4
Number of Cells in Straight Section	5
Number of Superperiods	2

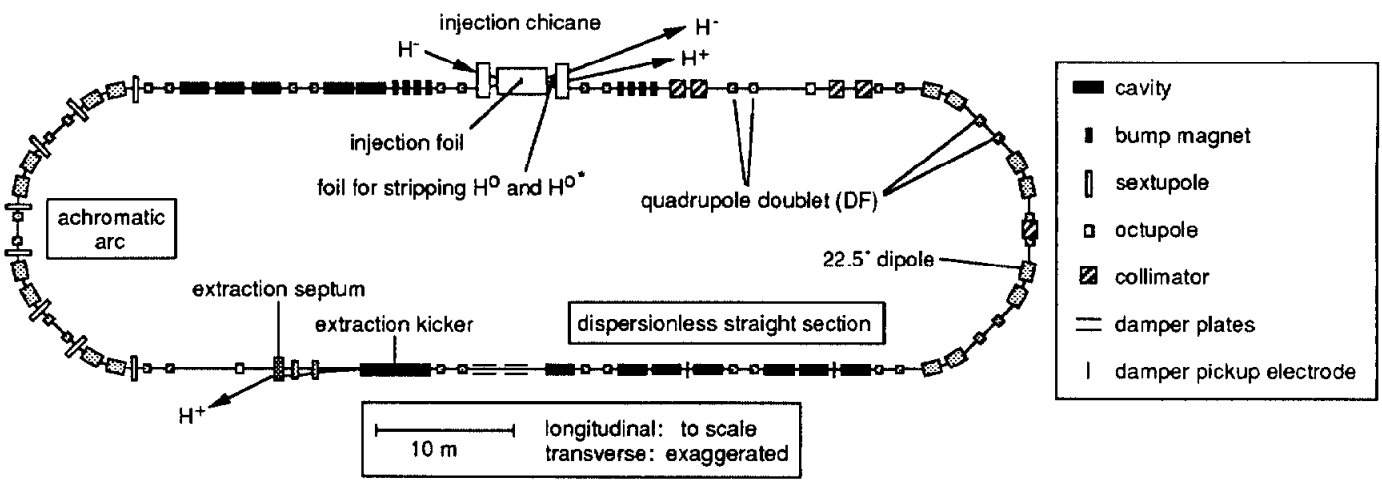

Figure 1. Ring layout.

*Work supported by the US Department of Energy, Office of Defense Programs.

0-7803-1203-1/93$03.00 © 1993 IEEE

it features dispersionless straight sections and arcs in the configuration of second-order achromats. Straight sections house the injection chicane, bump magnets for injection painting, collimators for beam-halo control, bunching cavities, a transverse-damper system, linear and nonlinear corrector elements, and the extraction kicker and extraction septum. One achromatic arc houses sextupoles, the other a dispersion collimator. Beam-position monitors and closed-orbit-correction steerers are located throughout the ring.

The desire to accomplish injection in a single drift mandated a minimum drift length of 8 m. This, together with arcs of the above-mentioned design, suggested a doublet, as opposed to a singlet, lattice. Five cells per straight section were chosen because of tune considerations, because for the required ring circumference the long drifts are adequately dimensioned (8.407 m), and because the five long drifts in low-loss areas (upstream of injection chicane and extraction kicker) can hold all rf cavities.

III. LINEAR LATTICE

The lattice functions of the ring, slightly different from those of one superperiod because of the injection chicane, are shown in Figure 2, the lattice parameters are given in Table 2. The machine tunes, $Q_x = 4.23$, $Q_y = 5.19$, correspond to phase advances per straight-section cell of 80.28° and 114.84°, respectively, near the value of 90° that minimizes aperture requirements. Stored-beam emittances are $\varepsilon_x = \varepsilon_y = 110$ π-mm-mrad to limit space-charge tune shifts to -0.15, thus remaining in a stable region of tune space. Apertures are dimensioned for transverse acceptances of 420 π-mm-mrad and a momentum acceptance of $\pm$ 1% $\delta p/p$. Ring dipoles and quadrupoles are described in Table 3.

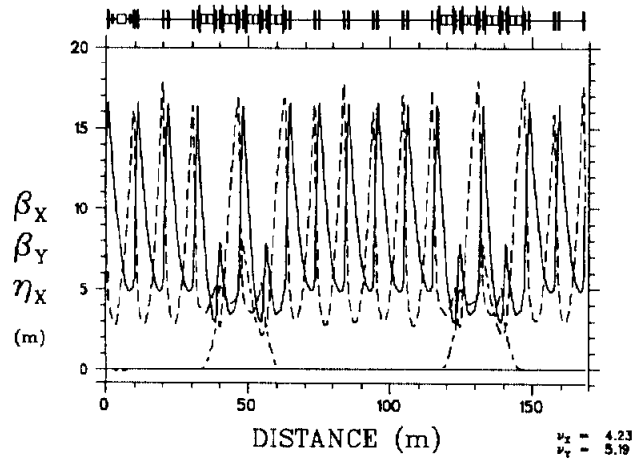

Figure 2. Ring lattice functions.

Table 2
Lattice Parameters

Q_x / Q_y	4.23 / 5.19
γ_T	3.34
$\beta_{x,max}$ (m) / $\beta_{y,max}$ (m)	16.62 / 17.93
$D_{x,max}$ (m)	7.70

Table 3
Magnet Description

Dipoles	
Arc Length (m)	1.600
Field (T)	1.188
Straight-Section Quadrupoles	
Effective Length (m)	0.500
Defocusing-Quadrupole Gradient (T/m)	−4.541
Focusing-Quadrupole Gradient (T/m)	3.990
Achromatic-Arc Quadrupoles	
Effective Length (m)	0.500
Defocusing-Quadrupole Gradient (T/m)	−3.687
Focusing-Quadrupole Gradient (T/m)	4.366

IV. NONLINEAR ISSUES

The first- and second-order chromaticities and the anharmonicities for the perfect ring, without either random or systematic errors in the magnetic elements, are given in Table 4. The beam will cover a large area in the tune diagram, both from the tune shift of the reference particle, due to space charge, and the tune spread around the central value, due to chromaticities and anharmonicities. Two families of four sextupoles each are placed in one arc to affect chromaticities. Two octupoles are placed at identical positions in the two ring straight sections to affect anharmonicities for control of tune spread.

Table 4
Nonlinear Ring Parameters

$\partial Q_x/\partial(\delta p/p)$	−4.86
$\partial Q_y/\partial(\delta p/p)$	−7.10
$\partial^2 Q_x/\partial(\delta p/p)^2$	182.07
$\partial^2 Q_y/\partial(\delta p/p)^2$	120.69
$\partial Q_x/\partial\varepsilon_x$ (π-m-rad)$^{-1}$	31.79
$\partial Q_y/\partial\varepsilon_y$ (π-m-rad)$^{-1}$	34.49
$\partial Q_x/\partial\varepsilon_y = \partial Q_y/\partial\varepsilon_x$ (π-m-rad)$^{-1}$	42.97

The widths of the resonance lines in the presence of ring imperfections, such as quadrupole-roll errors, and random and systematic higher-multipole errors in dipole and quadrupole fields, are a concern. Sets of Lambertson correctors are placed inside straight-section quadrupoles to affect the widths of the resonance lines. Skew-quadrupole correctors to affect $Q_x - Q_y = -1$, normal-octupole correctors to affect $4Q_x = 17$, and normal-decapole correctors to affect $Q_x + 4Q_y = 25$, $3Q_x + 2Q_y = 23$ and $5Q_x = 21$ have been identified.

V. RING INJECTION

The injection chicane, composed of two 5° septa and a 10° central dipole, moves the stored-beam orbit outward by 0.2 m. The injected H^- join the stored beam at the injection foil. Unstripped H^- are deflected away from the stored beam and disposed of in a beam dump, causing minimal activation in the ring.

Partially stripped H^{o*} (hydrogen atoms in excited states) have been identified as a source of activation in the Los Alamos Proton Storage Ring [2]. An H^{o*} loses its electron in a magnetic field of a strength that depends on quantum state. The H^{o*} thus may be stripped by a downstream magnet fringe field with consequent angular dispersion and particle loss. Placing the injection foil inside a dipole field can significantly reduce the problem by stripping higher states to remain within the stored-beam emittance. The field value is set so that lower states remain excited and can be disposed of in a beam dump after conversion to H^+ by a second foil. Optimization of this system indicates that a maximum loss of $<10^{-5}$ of the injected beam is in principle achievable.

Figure 3 illustrates the injection process. It shows the stored-beam ellipses of 110 π-mm-mrad area, and injected-beam ellipses of 3.2 π-mm-mrad (to 2σ) area. The injection point (•), namely x, x', y, y' of the injected-beam centroid, is stationary (although beam energy is swept by $\pm 0.33\%$ $\delta p/p$). It is chosen such that those H^{o*} that are deflected by <2 mrad before conversion to H^+ (some 99.9% of them) lie inside the stored-beam ellipse, as indicated by the shaded area in Figure 3.

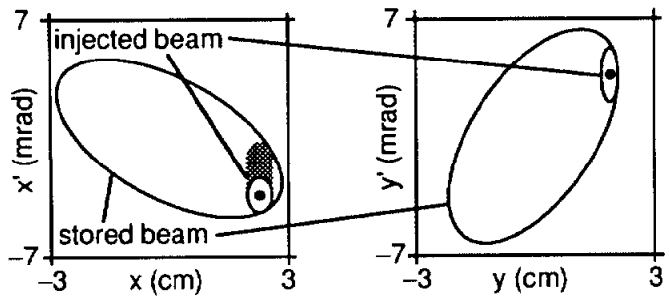

Figure 3. Transverse phase space at injection foil.

Injection painting is required to optimize the stored-beam distribution. Two sets of bump magnets relax the stored-beam centroid from near the injection point to the origin. Bumping is done such that emittance grows linearly with time. Because of the x-y correlation inherent in this bumping scheme, the distribution is rectangular and space-charge forces have octupolar components. This effect is magnified by an X-shaped beam pileup due to the particle motion in phase space. Figure 4 shows the transverse beam distribution at the end of injection, assuming accumulation in the perfect ring under neglect of space-charge forces. The foil is positioned so that its corner just covers the injected beam and injection painting keeps the number of foil traversals low, at an average of 10 per particle.

VI. PARTICLE TRACKING

The effects of space charge were assessed by first performing a fourth-order-polynomial fit to the potential of the distribution shown in Figure 4, and then tracking particles around the ring for 2000 turns including the forces derived from the potential. The beam-optics code Marylie [3] was used. Beam size increases but remains smaller than the physical aperture.

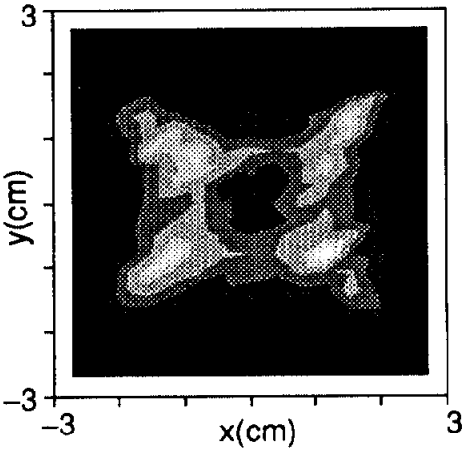

Figure 4. Beam distribution at end of injection.

The dynamic aperture of the machine was assessed by single-particle tracking to ninth order with the beam-optics code Tlie [4]. The machine was assumed to have random quadrupole-roll errors with a 10-mrad rms distribution, and random sextupole errors of 0.01 T/m^2 rms and decapole errors of 1.0 T/m^4 rms in the dipoles, as well as random octupole errors of 0.05 T/m^3 rms in the quadrupoles. The dynamic aperture as a function of particle momentum is shown in Figure 5. Improvements to the dynamic aperture will be made using first- and higher-order corrector elements.

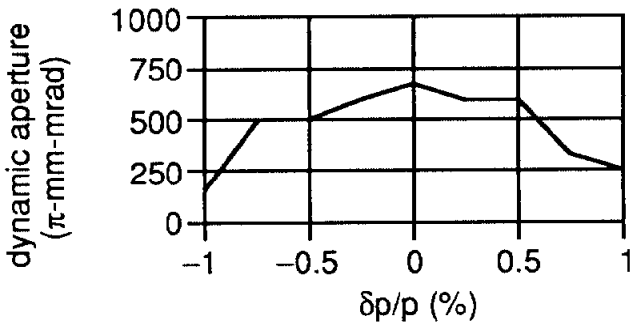

Figure 5. Dynamic aperture versus particle-momentum deviation.

VII. REFERENCES

[1] A. J. Jason, R. A. Hardekopf, R. W. Macek, H. A. Thiessen, and R. Woods, "A Los Alamos Design Study for a High-Power Neutron-Spallation-Source Driver," these proceedings.

[2] R. W. Macek, Los Alamos National Laboratory, private communication.

[3] A. J. Dragt, L. M. Healy, F. Neri, R. D. Ryne, D. R. Douglas, and E. Forest, "MARYLIE 3.0 – A Program for Nonlinear Analysis of Accelerator and Beamline Lattices," *IEEE Trans. Nucl. Sci.* 32(5), 2311 (1985).

[4] J. van Zeijts, "New Features in the Accelerator Design Code Tlie," to be published in the Proceedings of the Computational Accelerator Conference, Pleasanton, CA, Feb. 1993.